ACS APPLIED MATERIALS & INTERFACES

www.acsami.org

Research Article

Interface Engineering of "Clickable" Organic Electrochemical Transistors toward Biosensing Devices

Gonzalo E. Fenoy,* Roger Hasler, Christoph Lorenz, Jacopo Movilli, Waldemar A. Marmisollé, Omar Azzaroni,* Jurriaan Huskens, Peter Bäuerle, and Wolfgang Knoll*

Cite This: *ACS Appl. Mater. Interfaces* 2023, 15, 10885−10896

Read Online

ACCESS | Metrics & More | Article Recommendations | Supporting Information

ABSTRACT: "Clickable" organic electrochemical transistors (OECTs) allow the reliable and straightforward functionalization of electronic devices through the well-known click chemistry toolbox. In this work, we study various aspects of the click chemistry-based interface engineering of "clickable" OECTs. First, different channel architectures are investigated, showing that PEDOT-N_3 films can properly work as a channel of the transistors. Furthermore, the Cu(I)-catalyzed click reaction of ethynyl-ferrocene is studied under different reaction conditions, endowing the spatial control of the functionalization. The strain-promoted and catalyst-free cycloaddition of a dibenzocyclooctyne-derivatized poly-L-lysine (PLL-DBCO) is also performed on the OECTs and validated by a fiber optic (FO)-SPR setup. The further immobilization of an azido-modified HD22 aptamer yields OECT-based biosensors that are employed for the recognition of thrombin. Finally, their performance is evaluated against previously reported architectures, showing higher density of the immobilized HD22 aptamer, and originating similar K_D values and higher maximum signal change upon analyte recognition.

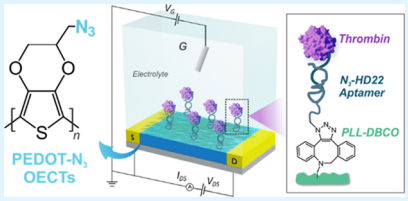

KEYWORDS: *organic electrochemical transistors, click chemistry, biosensors, thrombin, poly-L-lysine*

INTRODUCTION

Organic electrochemical transistors (OECTs) are a type of electronic device in which an organic semiconductor film bridges two electrodes (source and drain) and whose conductivity is modulated by the application of a gate voltage through an electrolyte.[1] These devices have been widely employed in the field of organic bioelectronics since they display many advantages over other transistor technologies such as metal oxide semiconductor field-effect transistors, including improved biocompatibility, long-term stability in aqueous environments, and higher transconductance (g_m).[2] In addition, compared to traditional neural recording electrodes, they offer higher signal-to-noise ratio and the possibility of fabricating compact arrays.[3,4] Therefore, multiple OECT-based bioelectronic devices have been developed in the last years such as biosensors, artificial synapses, and recording probes.[5−7]

Regarding the channel material of OECTs, poly(3,4-ethylenedioxythiophene) (PEDOT) and its water-stable colloidal complex with poly(styrenesulfonate) (PEDOT:PSS) have been the most employed polymers due to the high electronic conductivity of PEDOT and the excellent processability of PEDOT:PSS.[8,9] However, there are challenges that still need to be overcome; PEDOT's intrinsic doping yields devices with high threshold voltages (V_{TH}), meaning the necessity of high gate voltages to maintain the channel in the OFF state, therefore causing parasitic reactions with the electrolyte and prompting the deterioration of the devices.[10,11] Another major issue yet to surpass implies the interfacing of these materials with biological systems. In this regard, the functionalization of PEDOT is usually hindered by the lack of functional moieties in as-prepared films.[8,12] Likewise, the polyanion excess in PEDOT:PSS films limits their interactions with most biological elements (such as proteins, nucleic acids, and cells) since they present negative charges at physiological conditions.[13,14]

A particularly interesting approach to improve the biocompatibility and/or facilitate the functionalization of PEDOT (and PEDOT:PSS)-based films involves the derivatization of the EDOT monomer with a desired molecule/biorecognition element and its subsequent polymerization.[15,16] This method guarantees a high motif density in the film when homopolymers are desired, while the pristine EDOT monomer can also be blended to preserve a proper conductivity in the obtained film (since it is known that the incorporation of moieties to EDOT can diminish the conductivity of the resulting films[17]).[18] Therefore, numerous EDOT derivatives have been developed in the last years to facilitate the surface (bio)modification of these films, such as azido-EDOT (EDOT-N_3),[19] iminodiacetic acid-EDOT,[20] a cationic ammonium-modified EDOT,[16] and maleimide-EDOT,[21] among many others.[8,22] In this regard, we have recently reported the

Received: November 29, 2022
Accepted: January 30, 2023
Published: February 15, 2023

fabrication of PEDOT-N_3-based OECTs, endowing the incorporation of recognition units such as biotin and aptamers to the surface.[23]

On the other hand, click chemistry involves a group of orthogonal, selective, and high-yield reactions which can be performed at room temperature and in aqueous solvents, and whose relevance was recognized by the 2022 Chemistry Nobel Prize.[24,25] These reactions endow the efficient and straightforward fabrication of bio-constructs, being particularly relevant for bioconjugation and labeling purposes.[26,27] Among the different click reactions, the Cu(I)-catalyzed azide−alkyne cycloaddition (CuAAC) is certainly the most popular one.[28] The incorporation of the Cu(I) catalyst activates the alkyne moieties, facilitating the kinetics of the alkyne−azide condensation and also organizing the reacting groups, exclusively providing the 1,4-disubstituted 1,2,3-triazole.[29] These features have driven the application of CuAAC in a wide range of fields, and particularly toward the fabrication of interfacial architectures for the design of biosensing devices.[30,31] In addition, the strain-promoted alkyne−azide cycloaddition (SPAAC) reaction between ring-strained cycloalkynes and azides has also been widely applied for the catalyst-free modification of surfaces.[32,33] This reaction does not require the use of the copper, which is known to be cytotoxic, and can fully proceed under physiological conditions, increasing the possibilities for the engineering of surfaces though click chemistry.[34] In this context, researchers have employed CuAAC and SPAAC in order to develop several interfacial architectures that function as electrochemical and optical biosensing platforms.[31,35,36]

Similarly, the use of polyelectrolytes is a well-known approach for the functionalization of surfaces toward the development of organic bioelectronic devices.[11,37−39] Among them, poly-L-lysine (PLL) exhibits very interesting features, such as biocompatibility and hydrophilicity, making it particularly attractive for surface modification.[40] Furthermore, the addition of functional moieties to PLL has been recently explored, including different recognition elements such as biotin, maleimide, and RGD peptide.[40,41] In addition, oligo- and poly-ethylene glycol (OEG and PEG, respectively) chains have also been grafted to PLL, yielding a hydrogel-like brush structure while incorporating antifouling properties.[42] Very recently, the incorporation of both OEG and "clickable" dibenzocyclooctyne (DBCO) units to PLL was reported, allowing the SPAAC between these groups and probes that bear the complementary azide functionality and therefore endowing the controlled immobilization of DNA molecules to produce biosensing interfaces with antifouling features.[32,43]

In this work, we report the interface engineering of "clickable" OECTs in order to develop transistor-based biosensing devices. We first investigate different channel structures for PEDOT-N_3-based transistors. Furthermore, the CuAAC clicking of redox probes is studied under different conditions, providing insight into the spatial control of the functionalization process. Later, the Cu(I)-free click reaction of a DBCO-functionalized PLL is performed and studied by a fiber-optic surface plasmon resonance (FO-SPR) setup. The polyelectrolyte functionalization allows the further clicking of a thrombin-specific azide-derivatized HD22 aptamer, yielding thrombin sensing devices. Finally, the biosensing features of these transistors such as aptamer density, dissociation constant, and maximum response obtained are compared with previous reports.

EXPERIMENTAL SECTION

Reagents and Materials. Pyridine (99%), KCl, sodium dodecyl sulfate (SDS), acetonitrile (ACN), tetrabutylammonium hexafluorophosphate ($TBAPF_6$), 3,4-ethylenedioxythiophene (EDOT, 97%), dimethyl sulfoxide (DMSO), *n*-butanol (99.4%), acetone, tris[(1-benzyl-1*H*-1,2,3-triazol-4-yl)methyl]amine (TBTA, 97%), $CuSO_4 \cdot x5H_2O$, *tert*-butanol (*t*-butanol), sodium ascorbate (NaAsc), and *N*-(3-butynyl)phthalimide (*N*-But, 97%) were obtained from Sigma-Aldrich. Clevios C-B 54 V2 was obtained from Heraeus. Ethanol absolute (EtOH) was obtained from Merck. $HClO_4$ (20%) was obtained from Fluka. Phosphate-buffered saline (PBS) tablets were obtained from VWR. Ethynylferrocene (E-Fc, 97%) was obtained from abcr. Azido-ferrocene (N_3-Fc) was obtained from Baseclick GmbH. The azide (N_3)-modified thrombin-specific HD22 aptamer (N_3-HD22) (sequence 5′-/5AzideN-TTT-TTT-TTT-TAG-TCC-GTG-GTA-GGG-CAG-GTT-GGG-GTG-ACT-3′, M_w = 12.5 kDa) was custom-synthesized by Integrated DNA Technologies. Thrombin purified from human plasma (M_w = 37 kDa) was purchased from Enzo Life Sciences. All solutions were prepared with Milli-Q water. Au-interdigitated microelectrodes (IDE-3, 5/5 μm gap/electrode), a Ag/AgCl reference electrode (RE), a Pt counter electrode (CE), and a batch cell accessory were obtained from Micrux.

Electrochemistry Measurements. EIS and cyclic voltammetry (CV) experiments were performed with an Autolab potentiostat with both source and drain electrodes of the IDEs being connected as WE. For the aqueous measurements, an Ag/AgCl RE and a Pt wire as a CE were employed. Potentiostatic electrochemical impedance spectroscopy (EIS) measurements were performed in the frequency range from 0.1 to 10^5 Hz. For the organic solvent measurements, a Ag/Ag^+ electrode was used as a RE and a Pt wire as a CE. The electrolyte solution was 0.1 M $TBAF_6$ in ACN. The electrolyte was thoroughly bubbled with N_2 prior to the measurements.

Transistor Measurements. Transistor measurements were performed by means of a Keithley 4200-SCS probe station. For the transfer characteristics, the drain−source potential (V_{DS}) was kept fixed at −0.1 V. For the output characteristics, different gate voltages were employed in order to cover both ON and OFF states of the transistors, and they are reported in every plot (for instance, from −0.6 to 0.8 V, every 0.2 V). The V_{DS} was swept from 0 to 0.6 V. All the measurements were performed in 1× PBS.

Optical Microscope Measurements. Optical microscope images were obtained using an Olympus BX51M Microscope.

FO-SPR Measurements. Fiber optic probes (FO) were manufactured according to a previously reported procedure.[44] Briefly, TECS-clad step-index multimode fibers (Thorlabs Inc.), with a numerical aperture of 0.39 and a core diameter of 1000 μm, were cut to a length of 6.5 cm. At one end, a surface plasmon resonance (SPR)-sensitive zone (1 cm long) was fabricated by removing the jacket layer with a stripping tool and the cladding layer by dissolution in acetone. The SPR zone of the tip was subsequently cleaned with Milli-Q water and isopropanol and blow-dried under N_2. As-prepared tips were sputter-coated with 50 nm of gold and stored under argon until further use.

FO-SPR measurements were performed by optically connecting the tips to a Y-optical splitter via a commercially available bare fiber terminator (Thorlabs Inc.). Polychromatic light from a halogen light source (12 V, HL-2000-LL, Ocean Insight) was coupled into the input arm of the Y-optical splitter, guided to the fiber tip, back-reflected at the gold-coated cross section of the tip, and guided through the output arm of the splitter to a spectrometer (HR4000, Ocean Insight). The reflected light spectrum was normalized by the spectrum of the fiber in air before surface modification and processed by dedicated LabView software.

For the electropolymerization on the FO, the upper gold-coated part of the fiber was connected using a conductive copper tape (Reichelt Elektronik GmbH & Co. KG). To ensure electrical connection across the transition from the SPR zone to the upper gold-coated part of the fiber as well as a constant electrode area, a layer of conductive silver paint (RS Components Ltd) was applied

https://doi.org/10.1021/acsami.2c21493
ACS Appl. Mater. Interfaces 2023, 15, 10885−10896

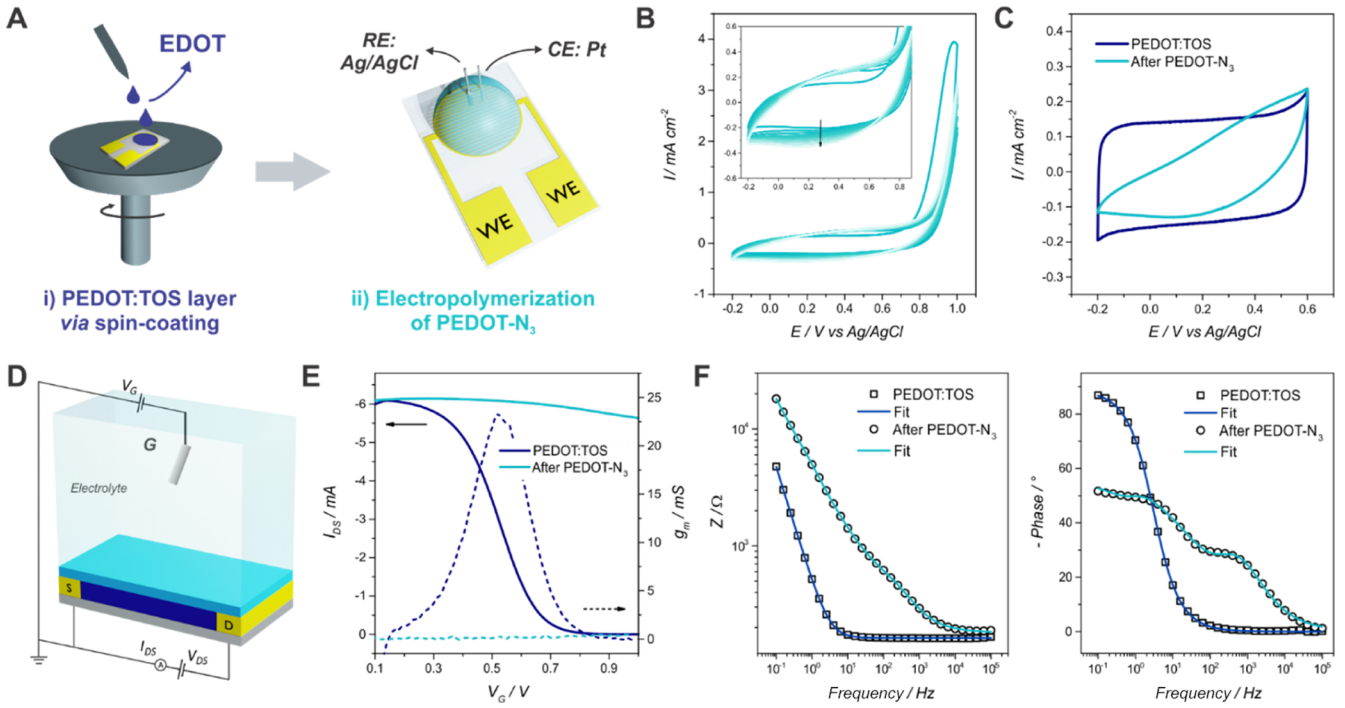

Figure 1. Scheme for the fabrication of the PEDOT:TOS-PEDOT-N_3 OECTs (A). Electropolymerization curves for the deposition of PEDOT-N_3 on PEDOT:TOS OECTs (0.1 M $HClO_4$, 10 mM EDOT-N_3, 0.1 M KCl, 0.05 M SDS, 40 mV/s, 10 cycles) (B). CV curves for a PEDOT-N_3 OECT (shorted D and S electrodes, 50 mV/s, 1× PBS) (C). Scheme of the structure and the measurement setup for the PEDOT-PEDOT-N_3 OECTs (D). Transfer characteristic curves (solid lines) and transconductance (dotted lines) for a PEDOT:TOS OECT before and after PEDOT-N_3 electropolymerization (V_{DS} = −0.1 V, 1× PBS) (E). EIS spectra for a PEDOT:TOS electrode before and after PEDOT-N_3 electropolymerization (1× PBS, 10 mV amplitude) (F).

and subsequently coated with a layer of liquid heat shrink tubing (Performix Liquid Tape, Plastidip, Plasti Dip Europe GmbH).

AFM Measurements. AFM measurements were performed in the tapping mode with a PicoPlus AFM microscope (Molecular Imaging, Agilent Technologies, Germany). PPP-NCHR-50 tips were employed (Nanosensors, Switzerland). The obtained images were processed with Gwyddion software (gwyddion.net).

Click Chemistry and Bioconjugation Protocols. The DMSO:-H_2O-based procedure for the clicking of *N*-But, E-Fc, and N_3-Fc molecules was performed as previously reported.[23] To this end, 4.5 μL of 1:2 $CuSO_4{\cdot}5H_2O$ 0.05 M and TBTA 0.05 M in 3:1 DMSO−*t*-butanol were mixed with 3 μL of 1 mM target molecule in DMSO, 4.11 μL of H_2O Milli-Q, 13.1 μL of DMSO, and finally 2.25 μL of NaAsc 0.1 M in Milli-Q and subsequently deposited on the modified area of the PEDOT-N_3 OECTs. Finally, the electrodes were thoroughly washed with DMSO, 3 M KCl, and Milli-Q water and blow-dried with N_2.

The clicking of the redox probe in EtOH was performed by adapting a previously reported protocol.[45] For the modification, the OECTs were immersed in a 1:1 EtOH/H_2O solution containing 3 mM E-Fc, 0.3 mM $CuSO_4$, and 1.5 mM NaAsc ($CuSO_4$ and NaAsc solutions were prepared in H_2O, while E-Fc was prepared in EtOH) for 4 h and rinsed with EtOH and Milli-Q.

The protocol for the modification with the dibenzocyclooctyl (DBCO)-functionalized poly-L-lysine (PLL) (PLL-DBCO) to PEDOT-N_3-FO was adapted from a previously reported protocol.[43] To this end, the polymer-modified FO was immersed in a 0.2 mg/mL PLL-DBCO solution in 1× PBS. For the PEDOT-N_3 OECTs modification, and based on the FO-SPR results, the transistors were immersed in the same solution for 60 min and rinsed with 1× PBS for 5 min.

For the clicking of the N_3-HD22 aptamer on the FO, a 2 μM N_3-HD22 1× PBS solution was employed. Next, and based on the FO-SPR results, the clicking of the N_3-HD22 aptamer on the PLL-modified OECTs was performed in an aqueous solution by immersing the electrodes in a 2 μM N_3-HD22 1× PBS solution by 60 min. The electrodes were subsequently rinsed with 1× PBS for 10 min.

For the recognition of thrombin by the HD22-modified FO, the thrombin solution was prepared in 1× PBS. Regarding the recognition of thrombin by the HD22-clicked transistors, the aptamer-modified transistors were incubated in the respective thrombin solution for 15 min (based on the FO-SPR results) rinsed with 1× PBS and dried with N_2.

Synthesis of EDOT-N_3. 2-Azidomethyl-2,3-dihydro-thieno[3,4-*b*][1,4]dioxine (EDOT-N_3) was synthesized according to a recently reported protocol.[19,23] Briefly, sodium azide was added to a solution of 2-chloromethyl-2,3-dihydro-thieno[3,4-*b*][1,4]dioxine (EDOT-Cl) in absolute DMF. The reaction mixture was heated to 120 °C for 3 h. After cooling, water was added to the reaction mixture, and the product was extracted with diethyl ether. The organic phases were combined, washed with water, brine, and dried over $MgSO_4$. Subsequently, diethyl ether was evaporated, and the crude product was purified over silica gel using petrol ether/ethyl acetate 95:5 as an eluent, yielding EDOT-N_3 as a colorless oil. The analytical data was in accordance with the literature data.[19]

Synthesis of PLL-DBCO. The PLL-DBCO polymer was synthesized according to a previously reported protocol.[43] Briefly, PLL (M_w 15−30 kDa) was functionalized in a one-step reaction, by mixing different molar ratios of NHS-$(OEG)_4$-methyl (without a functional group) and/or NHS-$(OEG)_4$-DBCO (Figure S1).

RESULTS AND DISCUSSION

Optimization of the Channel Architecture. We first investigated different channel architectures for the "clickable" OECTs. We essayed the fabrication of a transistor made of two layers, in which the lower layer is made of the conducting polymer PEDOT with tosylate as a dopant (PEDOT:TOS), while the top one is composed of PEDOT-N_3, thus providing the channel with "clickable" azide moieties. To this end,

https://doi.org/10.1021/acsami.2c21493
ACS Appl. Mater. Interfaces 2023, 15, 10885−10896

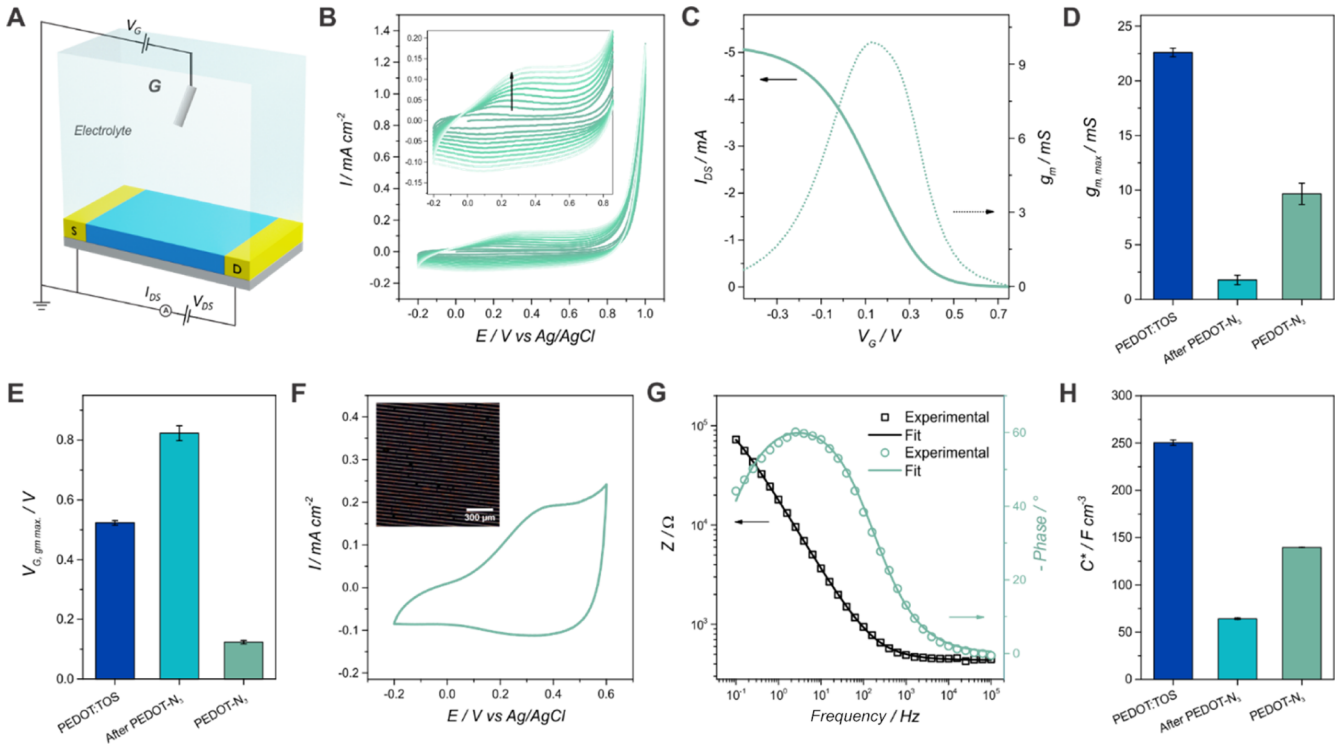

Figure 2. Scheme for the PEDOT-N_3 OECTs (A). Electropolymerization curves for a PEDOT-N_3 OECT (0.1 M $HClO_4$, 10 mM EDOT-N_3, 0.1 M KCl, 0.05 M SDS 0.05 M, 40 mV/s, and 10 cycles) (B). Transfer characteristic curves and transconductance for a PEDOT-N_3 OECT (V_{DS} = −0.1 V, 1× PBS) (C). $V_{G,g_{m,max}}$ (D) and $g_{m,max}$ (E) obtained values for both OECT fabrication strategies. CV curves for a PEDOT-N_3 OECT (shorted D and S electrodes, 50 mV/s, 1× PBS). The inset shows an optical micrograph of a PEDOT-N_3 OECT (F). EIS spectrum and fitting for a PEDOT-N_3 electrode (1× PBS, 10 mV amplitude) (G). Volumetric capacitance obtained from CV curves for both fabrication approaches (H).

PEDOT:TOS OECTs were fabricated according to a previously reported protocol by in situ chemical polymerization on commercial interdigitated electrodes (IDEs) by spin coating (Figure 1A).[11] The elevated conductivity of PEDOT:TOS provides the transistors with very high transconductance values, while the fabrication method remains simple and reproducible (a box plot for the resistance values obtained for a set of transistors is shown in Figure S2).[11] Next, a layer of PEDOT-N_3 was electropolymerized from an aqueous solution on top of the PEDOT:TOS OECTs, as shown in Figure 1A (to this end, both S and D electrodes of the OECT were connected as WE, as well as for all the further CV measurements). The electropolymerization curves show that the deposition of the film takes place successfully, showing similar features as those previously reported for the deposition of PEDOT-N_3 on different substrates (Figure 1B).[23,35] In addition, CV measurements show that the deposition of the PEDOT-N_3 layer originates a significant change in the response of the conducting polymer electrodes (Figures 1C and S3), shifting from the typical capacitive-like behavior of PEDOT-based electrodes to a more resistive character.[11,46] This result can be ascribed to the lower conductivity of the azido-bearing polymer compared to that of PEDOT:TOS, in agreement with previously reported results.[18]

Next, by making use of an electrolyte-gated configuration (Figure 1D), the transfer characteristics of the PEDOT:TOS OECTs before and after PEDOT-N_3 modification were evaluated. From Figure 1E, it can be noticed that PEDOT:TOS transistors exhibit the typical depletion mode, *i.e.*, in the absence of a gate voltage, they display the ON state. More interestingly, the deposition of the PEDOT-N_3 layer causes a strong diminution of the current modulation features of the transistor, which is observed as a clear reduction in the transconductance values. This behavior can be ascribed to the lower conductivity of the PEDOT-N_3 film as well as to some extent of the transport blocking effect, in line with the results observed by CV.[18,23] In order to corroborate that the outcomes observed were due to the deposition of the PEDOT-N_3 layer and not to some degradation caused by the cycling of the PEDOT:TOS electrode in the acidic electropolymerization medium, a control experiment was performed by cycling the PEDOT:TOS OECT in the electropolymerization solution without the EDOT-N_3 monomer (Figure S4). No significant changes appear after the cycling, meaning that the observed effects are due to the deposition of the PEDOT-N_3 layer.

Next, with the aim of gaining further insights into the processes taking place in the conducting polymer films, electrochemical impedance spectroscopy (EIS) measurements were performed for the PEDOT:TOS electrodes before and after the deposition of the PEDOT-N_3 layer (Figures 1F and S5). It is observed that the modification of the PEDOT:TOS film with PEDOT-N_3 causes a high increase in the impedance of the electrodes, in agreement with the results derived from CV and FETs measurements. In addition, the phase angle at intermediate frequencies (~10^2 to 10^3 Hz) increases compared to that of PEDOT:TOS, indicating the presence of a second capacitive element. Further discussion and details of the EIS response are presented in the Supporting Information.

In addition, the clicking of an acetylene-modified *N*(3-butynyl)phthalimide was performed on the two-layer transistors in order to evaluate their performance after the click

https://doi.org/10.1021/acsami.2c21493
ACS Appl. Mater. Interfaces 2023, 15, 10885−10896

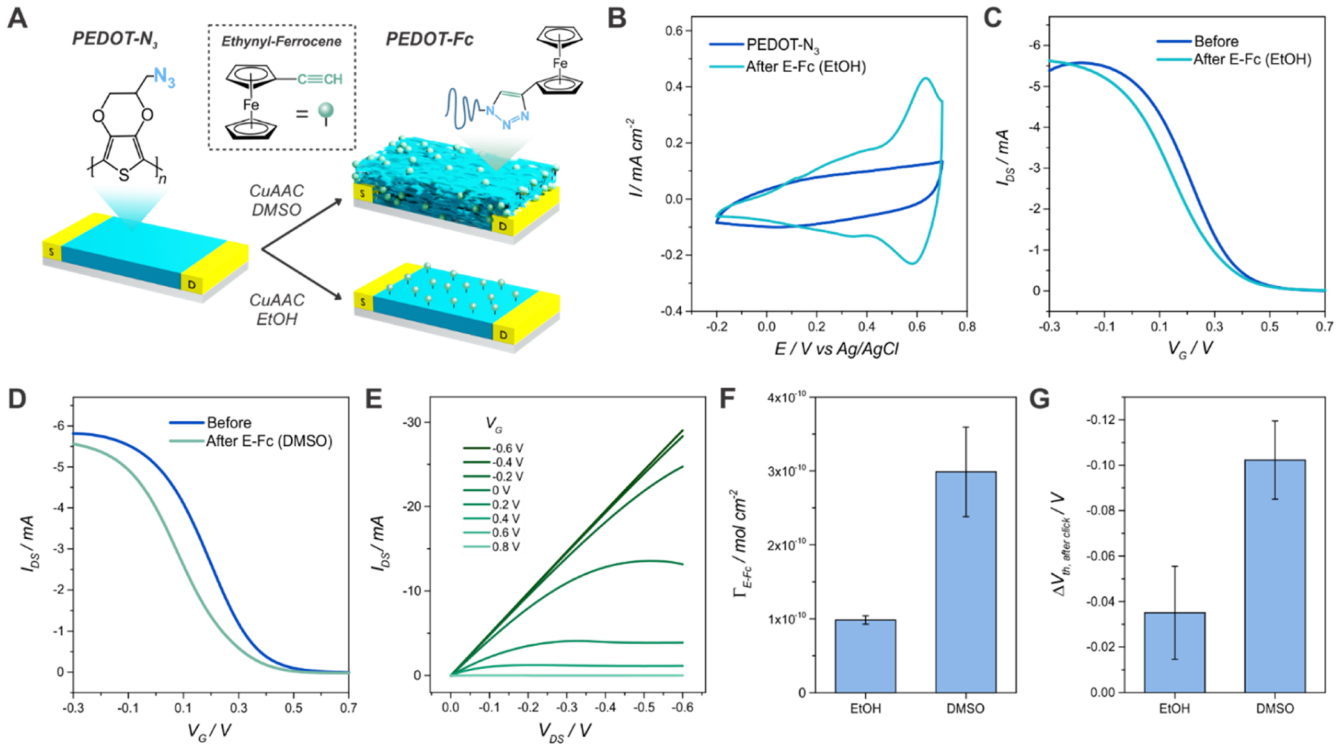

Figure 3. Scheme for the click functionalization of the PEDOT-N_3 OECTs with ethynyl-ferrocene employing two different approaches (A). CV curves (B) and transfer characteristics (C) for a PEDOT-N_3 electrode before and after the click reaction with E-Fc in EtOH (CV: 50 mV/s, OECTs: V_{DS} = −0.1 V, 1× PBS). Transfer characteristics for a PEDOT-N_3 electrode before and after the click reaction with E-Fc in DMSO (V_{DS} = −0.1 V, 1× PBS) (D). Output characteristic curves for a PEDOT-N_3 OECT after the click reaction with E-Fc in DMSO (1× PBS) (E). Shift in the threshold voltage (F) and density of clicked molecules (G) upon the clicking of E-Fc for both EtOH and DMSO-based approaches.

reaction. The devices showed an abrupt diminution of the current values after the modification process, meaning that the performance of the transistor was negatively affected (Figure S6).

Therefore, and as an alternative to obtain "clickable" OECTs with proper functioning before and after the clicking process, we performed the direct electropolymerization of PEDOT-N_3 on the Au IDEs (Figure 2A). It has been reported that relatively weak electrical fields lead to the formation of thin films that can properly work as a channel of OECTs.[23,47,48] The curves for the electropolymerization are shown in Figure 2B, exhibiting similar values for the current density as those previously reported.[23] Moreover, optical microscope pictures as well as AFM measurements of the PEDOT-N_3 OECTs confirm the deposition of homogeneous and smooth films (inset of Figures 2F and S8).

The evaluation of the transfer characteristics of the transistors (Figure 2C) yielded devices with lower maximum transconductance and threshold voltages than the PEDOT:TOS ones (Figures 2D and S7). Similarly, compared to the transistors fabricated with the two layers (Figure 2E), these devices showed significantly lower maximum transconductance voltages ($V_{G,g_{m,max}}$) and higher g_m. Obtaining transistors with $V_{G,g_{m,max}}$ values close to 0 V allows the development of highly energy-efficient devices while diminishing parasitic reactions and the alteration of biomolecules when they are biased at this V_G.[9,11,49] In addition, high g_m values endow the development of sensitive OECT-based biosensing devices.[11,49]

CV and EIS measurements were performed in order to electrochemically characterize these transistors/electrodes (Figure 2F,G). The impedance response shows significantly higher impedance than PEDOT:TOS electrodes, ascribed to the high electronic/charge-transfer resistance of the PEDOT-N_3 along the conducting polymer domains, as expected from the lower conductivity of the azido-derivatized obtained film.[18] Further description of the EIS response can be found in the Supporting Information.

The CV curves of the PEDOT-N_3 electrodes show very similar features as those seen for the PEDOT:TOS-PEDOT-N_3 ones, meaning that the response is dominated by the PEDOT-N_3 in both cases. Figure 2H shows the comparison of the volumetric capacitance obtained from the CV curves for the different architectures. It is observed that the devices fabricated only with PEDOT:TOS as channel show significantly higher volumetric capacitance than after the modification with the PEDOT-N_3 film and also than those composed of only the PEDOT-N_3 polymer as channel, as expected due to the higher conductivity of the PEDOT:TOS polymer.[18,19]

Summarizing, it is observed that the different architectures have a strong impact on the electrochemical and electrical response of the transistors. When a PEDOT-N_3 layer is electropolymerized on top of a highly conducting PEDOT:TOS layer, it acts as a blocking membrane. However, it allows the mixed ionic electronic transport to happen when working as a single channel film between the IDEs. Next, this fabrication method is chosen to perform the clicking of different molecules to the transistors.

Clicking of Redox Probes and PLL-DBCO. In order to corroborate the presence and accessibility of the azide moieties of the "clickable" OECTs, the copper(I)-catalyzed click reaction of an ethynyl-derivatized ferrocene (E-Fc) was performed (Figure 3A). Two different protocols were

https://doi.org/10.1021/acsami.2c21493
ACS Appl. Mater. Interfaces 2023, 15, 10885−10896

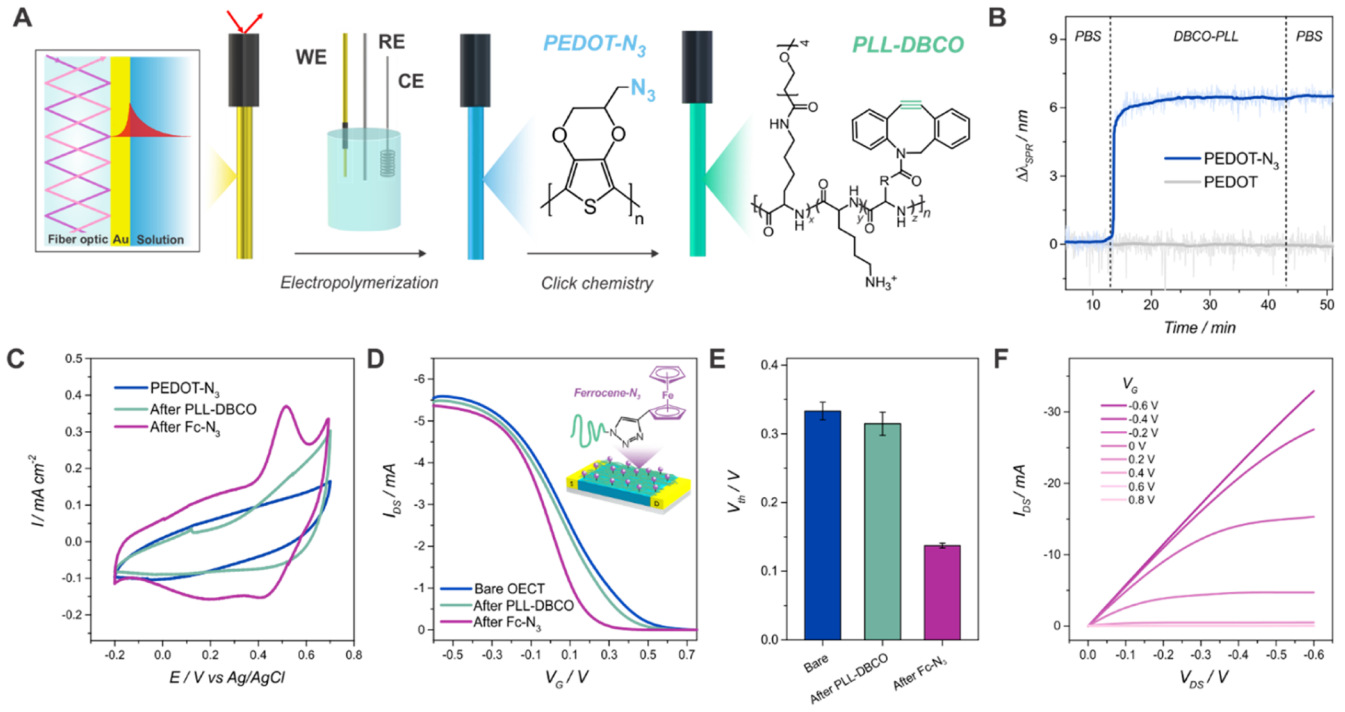

Figure 4. Scheme of the FO-SPR setup and the steps involved for the "click"-based functionalization of the fibers (A). Kinetic experiment for the clicking of PLL-DBCO to a PEDOT-N_3-FO (raw and smoothed data) (B). CV curves for a PEDOT-N_3 electrode before and after the clicking of PLL-DBCO and N_3-Fc (50 mV/s, 1× PBS) (C). Transfer characteristic curves (D) and threshold voltage (E) for a PEDOT-N_3 OECT before and after the clicking of PLL-DBCO and N_3-Fc (V_{DS} = −0.1 V, 1× PBS, n = 3). Output characteristic curves for a PEDOT-N_3 OECT after the click reaction with PLL-DBCO and N_3-Fc (1× PBS) (F).

investigated for the click process: (i) a DMSO/H_2O-based and (ii) an EtOH/H_2O-based protocol. It has been previously reported that solvent composition can direct the click functionalization of PEDOT-N_3 films.[50] In this regard, DMSO promotes the swelling of PEDOT-N_3, thus allowing the bulk functionalization of the polymeric films. On the other hand, other solvents such as water limit the spatial extent of the click reaction, and therefore different densities of functionalized groups are expected when employing different solvents.

Due to the low solubility of E-Fc in water, the redox probe was dissolved in EtOH and, therefore, the clicking process was performed in an EtOH/H_2O mixture, adapting a previously reported protocol.[45] Figure 3B shows the CV curves of a PEDOT-N_3 OECT connected as a single electrode before and after the clicking of E-Fc in EtOH (a blank experiment for the clicking of E-Fc employing PEDOT electrodes with no azide moieties obtained under the same conditions is shown in Figure S11, confirming the necessity of the azide moieties for the reaction to occur). The redox peaks of the ferrocene/ferricenium (Fc/Fc^+) couple are observed at ∼0.61 V (0.63 for the anodic sweep and 0.58 for the cathodic one), confirming the successful clicking of the redox probe. The observed redox potential is higher than that obtained for the clicking of E-Fc while employing DMSO as a solvent (0.51 V).[23] This effect could be attributed to a hindered charge transport from the redox probes throughout the film and to the contact electrodes since they are supposed to be located closer to the surface of the OECTs when the clicking process is performed in EtOH/H_2O.[51,52] In this sense, the DMSO-induced swelling allows the clicking of the Fc molecules also inside the film and, therefore, closer to the Au electrodes, facilitating the electron hopping mechanism through a shorter distance and diminishing the effective potential at which the redox couple is observed.

The analysis of the transfer characteristics also gives further information in this regard (Figure 3C,D). When the click reaction is performed in DMSO/H_2O, the shift of the threshold voltage caused by the functionalization with the redox probe is higher than that observed for the EtOH-based reaction (Figure 3F). A shift of −100 mV is observed for the DMSO-based clicking reaction, while the EtOH-based protocol yields a shift of only −35 mV (the absolute values are shown in Figure S9). This result supports the hypothesis of the DMSO-induced swelling, which causes a more porous structure, and, therefore, additional ion transport channels that facilitate the redox process throughout the film, as previously reported.[11,50] A blank experiment for the OECT functionalization with E-Fc using PEDOT OECTs without azide moieties is reported in Figure S11, showing no shift in V_{TH}.

The density of clicked E-Fc molecules was estimated from the CV measurements, according to $\Gamma = Q/nFA$, where Q is the integrated charge of the redox peaks, n is the number of electrons transferred (n = 1), F is the Faraday constant, and A is the electroactive surface area of the electrode (9.62 mm^2). Next, a significantly higher density of clicked redox molecules is observed when the clicking process is performed in DMSO than when using EtOH as a solvent (($\Gamma = 3.0 \pm 0.6) \times 10^{-10}$ mol cm^{-2} vs ($\Gamma = 9.8 \pm 0.6) \times 10^{-11}$ mol cm^{-2}), Figure 3G. These results also support the hypothesis of the DMSO-induced swelling, which increases the amount of reachable azide moieties compared to the EtOH-based click reaction, and thus allows a "bulk" clicking of the E-Fc. A scheme is shown in Figure 3A.

https://doi.org/10.1021/acsami.2c21493
ACS Appl. Mater. Interfaces 2023, 15, 10885−10896

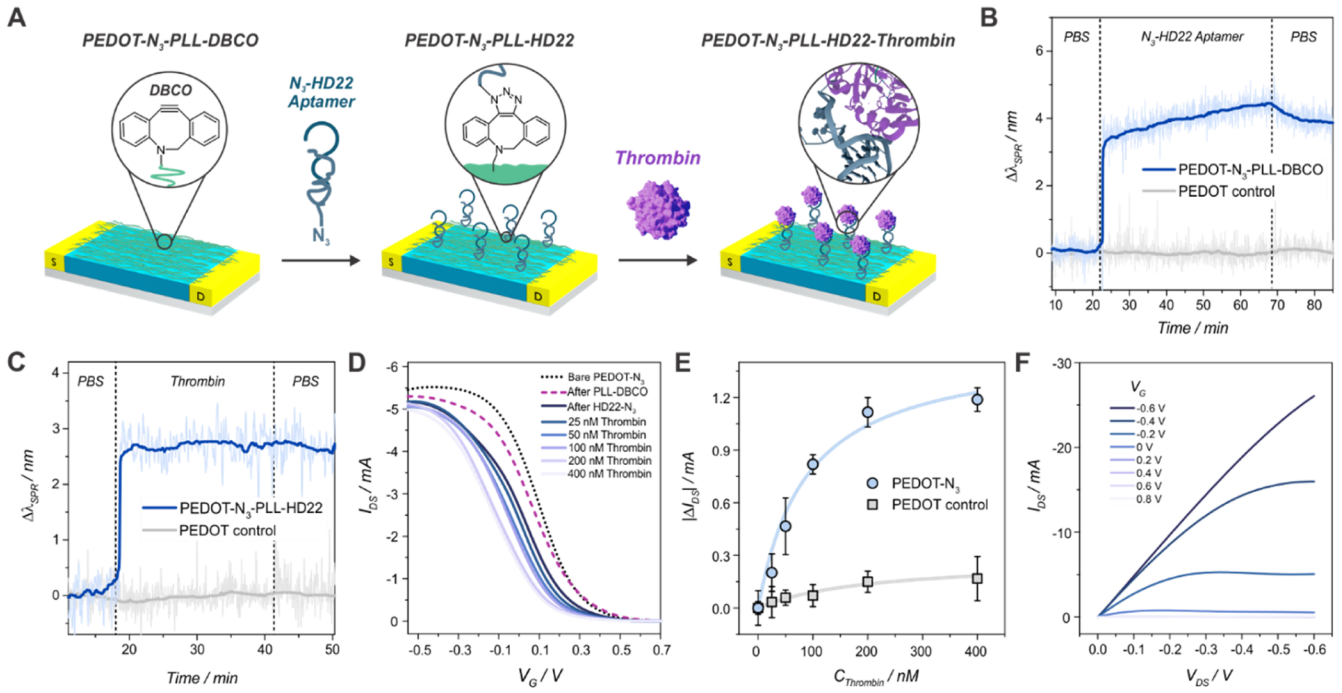

Figure 5. Scheme of the fabrication of the thrombin biosensors based on "clickable" OECTs (A). FO-SPR kinetic experiment for the clicking of the N_3-HD22 aptamer to a PLL-DBCO-functionalized PEDOT-N_3-FO (raw and smoothed data) (B). FO-SPR kinetic experiment by the recognition of thrombin by the aptamer-modified FO (C). Transfer characteristic curves of a PEDOT-N_3 OECT before and after PLL-DBCO and N_3-HD22 functionalization and further thrombin recognition (V_{DS} = −0.1 V, 1× PBS) (D). Change in the drain−source current obtained from the transfer characteristics for a PEDOT-N3-HD22 OECT and control experiment with a PEDOT OECT (three measurements) (E). Output characteristic curves for a HD22-PLL-PEDOT-N_3 OECT after the recognition of 400 nM thrombin (1× PBS) (F).

Finally, the output curves show that the transistors are fully operational after the clicking procedure and the different electrochemical cycling procedures in PBS in both solvents, probing their robustness and stability (Figures 3E and S10). Interestingly, the possibility of employing different clicking protocols provides the opportunity of directing and tuning the density of clicked molecules very easily by properly choosing the reaction conditions.

Next, the clicking of a dibenzocyclooctyl (DBCO)-functionalized poly-L-lysine (PLL) (PLL-DBCO) to the PEDOT-N_3 OECTs was performed. To this end, PLL was firstly grafted with oligo(ethylene glycol) (OEG) units and DBCO functional moieties according to a previously reported protocol (Figures 4A and S1).[43] The DBCO residues allow for the fast, catalyst-free, and bio-orthogonal clicking of azido-derivatized counterparts, while OEG moieties are known to decrease unspecific binding. In this regard, the surface immobilization of PLL-DBCO has been reported to endow a rapid and specific anchoring of DNA molecules using click chemistry, providing a precise control of the probe density.[43]

Next, the clicking of PLL-DBCO to PEDOT-N_3 was investigated by employing a FO-SPR setup. To this end, films of PEDOT-N_3 were electropolymerized on Au-coated optical fibers (FO) by using the same protocol employed for the fabrication of the OECTs (while connecting the gold-coated FO as a WE, Figure 4A). The electropolymerization of the PEDOT-N_3 film on the FO shows very similar characteristics to those observed for the procedure on the IDEs (Figure S12), validating the approach. A further discussion is presented in the Supporting Information. Next, the functionalization with PLL-DBCO in PBS was studied by tracking the resonance wavelength over time. From Figure 4B, it can be observed that the incorporation of PLL-DBCO causes a shift in the resonance wavelength toward higher values, implying the effective reaction of the functionalized polyelectrolyte and the azido-bearing surface. The reaction achieves a plateau in less than 20 min, in close agreement with previously reported results.[43] Furthermore, a shift of 6.5 ± 0.2 nm is observed, which can be associated with a surface mass density of 349 ± 19 ng/cm^2 (see the Supporting Information).[42] In this sense, the obtained surface mass density of grafted PLL-DBCO is considerably higher than that reported for the adsorption of the same material on Au surfaces (without employing the click reaction, yielding very thin films).[43] We believe that this result can have two origins. On the one hand, it has been reported that the adsorption of modified PLL polyelectrolytes on Au/Si negatively charged surfaces can be hindered when replacing the amino moieties with other functional ones such as OEG or DBCO, thus diminishing the electrostatic interactions between the surface and the polymer and yielding thinner and weakly bound layers.[42,53,54] Moreover, the PEDOT-N_3 film shows a higher rugosity compared to bare Si or Au surfaces, thus providing more binding sites for the stable and efficient clicking of a thicker layer of PLL-DBCO. Therefore, the developed "grafting-to" approach of PLL-DBCO to the PEDOT-N_3 film yields a much thicker PLL layer, and thus many DBCO moieties remain accessible for the further click reaction.

The control experiments, performed by executing the same steps for the FO modification with a PEDOT film without azide moieties (Figure S13), confirmed the specificity of the modification reaction and the absence of nonspecific binding (Figure 4B).

https://doi.org/10.1021/acsami.2c21493
ACS Appl. Mater. Interfaces 2023, 15, 10885−10896

Next, the same functionalization process was performed on the PEDOT-N_3 OECTs and studied by CV measurements, as shown in Figure 4C. From the CV curves, it can be observed that the capacitance of the electrode upon the modified-PLL clicking increases by 16%. This result is ascribed to the incorporation of the charged polyelectrolyte on the conducting polymer electrode and is in line with previous reports since the deposition of polyelectrolytes is known to increase the double-layer capacitance of conducting polymer electrodes.[46,55,56]

In addition, the clicking of an azido-derivatized ferrocene (N_3-Fc) to the PLL-DBCO modified electrode was performed, and the process was studied via CV measurements. Figure 4C shows that the peaks of the redox couple can be observed after the clicking procedure, confirming that some DBCO moieties remain accessible after the PLL-DBCO clicking to the PEDOT-N_3 electrode. Next, the density of the clicked N_3-Fc molecules was estimated from the CV curves, yielding a value of $(\Gamma = 1.1 \pm 0.4) \times 10^{-10}$ mol cm^{-2}. Compared to the previously reported clicking of N_3-modified DNA probes to PLL-DBCO adsorbed on Au surfaces,[43] this value is considerably higher, reinforcing the hypothesis of the obtention of a thicker PLL-DBCO film via click chemistry to PEDOT-N_3 that bears more accessible DBCO moieties for further functionalization.

The next step involved the study of the clicking of the PLL-DBCO to PEDOT-N_3 OECTs, as displayed in Figure 4D. Upon the functionalization process, a small shift of the threshold voltage of ≈20 mV toward more negative potentials is observed, which is in line with the results observed for the clicking of E-Fc in EtOH. The further clicking of N_3-Fc (performed in DMSO) causes a higher negative shift of a threshold voltage of ∼180 mV, also supporting the previously indicated hypothesis. In addition, the output characteristics of the OECTs after both modification processes (Figure 4F) shows that the transistors preserve their features as amplification devices, thus demonstrating their excellent stability after the modification procedures.

Thrombin Biosensor Fabrication and Benchmarking. Next, the PLL-DBCO-functionalized PEDOT-N_3 OECTs were employed to construct thrombin aptamer-based biosensors. To this end, an azide-derivatized HD22 aptamer (sequence 5′-/5AzideN-TTT-TTT-TTT-TAG-TCC-GTG-GTA-GGG-CAG-GTT-GGG-GTG-ACT-3′), known to interact with the exosite II of thrombin,[57] was immobilized to the OECTs via the Cu(I)-free strain-promoted click reaction. The importance of detecting thrombin roots in its crucial role in hemostasis, being responsible for the conversion of fibrinogen into fibrin for the development of blood clots.[58] Since imbalances in coagulation can lead to various pathologies such as heart attack, stroke and thrombosis, and pulmonary embolism, among many others,[59,60] the quantitative detection of this protein is of high clinical relevance.

We first evaluated the strain-promoted Cu(I)-free clicking of the N_3-HD22 aptamer to PLL-DBCO-modified PEDOT-N_3 via the FO-SPR setup. To this end, PEDOT-N_3 was electropolymerized on FO, the functionalization with PLL-DBCO was performed, and the clicking of the N_3-HD22 aptamer was studied in a kinetic experiment (Figure 5B). It can be seen that the binding of the aptamer to the PLL-modified polymer yields a shift of the resonance wavelength of 3.9 ± 0.3 nm, equivalent to a surface mass density of 199 ± 16 ng/cm^2. Compared to previously reported surface architectures for HD22 immobilization such as poly(HPMA-*co*-CBMAA) brushes,[61] or NeutrAvidin OEG-biotin self-assembled monolayers,[44] this method yields a substantial increase in the surface mass density of anchored HD22.

In addition, and similar to what was reported for the click of N_3-Fc, the obtained density of clicked N_3-HD22 is higher compared with the amount of clicked N_3-modified DNA probes to PLL-DBCO adsorbed on Au surfaces.[43] Therefore, the "grafting-to" approach for the clicking of PLL-DBCO to PEDOT-N_3 films yields a thicker and "clickable" polymeric interface with accessible DBCO moieties for further clicking.

As a control experiment, PEDOT (without azide moieties) was electropolymerized on a FO and subjected to the same treatment than PEDOT-N_3, *i.e.*, the functionalization with PLL-DBCO. Later, no unspecific adsorption of the aptamer to the PEDOT film was observed (Figure 5B).

Subsequently, the recognition of thrombin by the aptamer-modified fiber optic was essayed. From Figure 5C, it can be observed that the immersion of the HD22-PLL-PEDOT-N_3-fiber in a 200 nM thrombin solution in PBS, and its further washing step yields a shift in the resonant wavelength of 2.7 ± 0.4 nm ascribed to the recognition of the cardiac biomarker by the HD22-modified fiber optic. This shift can be associated with a surface mass density of thrombin of 151 ± 22 ng/cm^2. In this regard, the specificity of HD22 toward thrombin is well-documented, binding to the exosite II of thrombin,[57] and SPR measurements have shown that HD22 does not bind to human serum albumin, human immunoglobulin G, nor prothrombin.[61] In contrast, HD1, another well-known thrombin-specific aptamer, binds to thrombin via exosite I and II, and it also binds to prothrombin with a K_D value of 37 nM.[61]

Moreover, the blank experiment employing a PEDOT-modified FO previously treated with the same conditions for the aptamer binding showed no thrombin unspecific adsorption, corroborating the specificity of the engineered surface.

Next, the detection of thrombin was also assessed by the PEDOT-N_3 transistors. To this end, PEDOT-N_3 OECTs were first functionalized with the PLL-DBCO polymer. Subsequently, the N_3-HD22 aptamer was clicked to the surface, and finally, the sensors were incubated for 15 min in the respective thrombin solutions. The transfer characteristic curves were measured after each functionalization and incubation step, and they are shown in Figure 5D. It can be observed that the clicking of the HD-22 aptamer to the PLL-DBCO OECTs causes a shift in the V_{TH} to more negative potentials of 34 mV, in line with previous reports.[23]

Furthermore, it is noticed that the recognition of thrombin by the HD22-modified surface also yields a negative shift of the threshold voltage, which can be seen as a reduction of the registered drain−source current when processing the values at a fixed V_G. This effect has been previously reported for organic transistors, and it has been ascribed to the generation of negative charges in the semiconductor channel by the positively charged thrombin.[62] Later, the I_{DS} values displayed at V_G = 0 V were obtained and fitted to a Hill (n = 1) adsorption model in order to obtain an apparent K_D for the interfacial architecture assembled. The K_D value for the HD22-PLL-DBCO-functionalized OECTs is 88 ± 20 nM (R^2 = 0.98), in line with previous reports.[57,63] In addition, a LOD of 22 nM was obtained as 3 times the standard deviation of the blank measurement.

In order to evaluate the specificity of the developed OECT-based thrombin sensors, PEDOT-based transistors were

https://doi.org/10.1021/acsami.2c21493
ACS Appl. Mater. Interfaces 2023, 15, 10885−10896

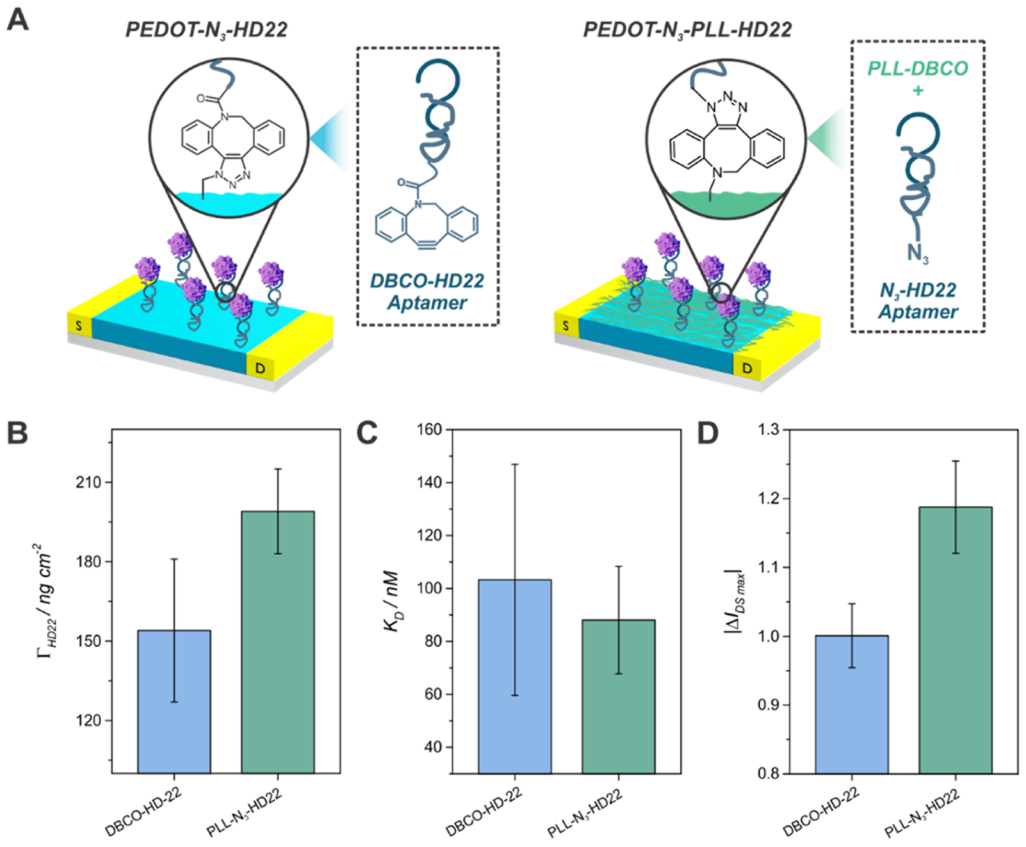

Figure 6. Scheme of the interfacial architecture of both PEDOT-N_3 OECTs-based thrombin biosensing devices (A). Mass density of anchored aptamers for both approaches obtained from FO-SPR measurements (B). Dissociation constant value comparison for both sensing architectures (C). Maximum change in I_{DS} registered for the recognition of thrombin for both OECT-based biosensors (D). Data for PEDOT-N_3-HD22 was taken from ref 23.

fabricated by using the same production protocol (see Figure S14), and an identical functionalization process as that performed for the PEDOT-N_3 transistors was followed (i.e., functionalization with PLL-DBCO, N_3-HD22, and finally thrombin). The acquired I_{DS} values from the transfer characteristics of the transistors (Figure 5E) for the different thrombin concentrations yielded almost no change, verifying the specificity of the PEDOT-N_3-based biosensing devices and the absence of signal ascribed to nonspecific binding. In this regard, some nonspecific adsorption of thrombin could be expected and might trigger a sensing response on the control OECTs (which can be actually observed as a small change in the registered I_{DS}, Figure 5E). However, the thrombin is positively charged at the working pH, and since the PEDOT backbone is known to bear positive charges in the doped state,[11,17] this would minimize the nonspecific thrombin adsorption on the control PEDOT OECTs. Next, the specific interaction between the HD22 aptamer and thrombin is stronger and results in an easily measurable difference on the transfer characteristics when detecting the binding. Finally, the output characteristics of the functionalized PEDOT-N_3 OECTs were obtained after the detection of 400 nM thrombin, accounting for the excellent stability of the biosensing devices (Figure 5F).

Finally, we compared the performance of the developed interfacial sensing architecture with that formerly reported also based on "clickable" OECTs (Figure 6A).[23] Very recently, PEDOT-N_3 OECT-based biosensing devices were fabricated by clicking a DBCO-bearing HD22 aptamer (DBCO-HD22) via SPAAC to azido-bearing organic transistors. To the best of our knowledge, this is the only previous report on OECT-based biosensors for thrombin detection (while other FET-based biosensing devices have also been developed during the last years for the monitoring of thrombin, and a comparison is presented in Table S4 of the Supporting Information).

First, the mass density of immobilized aptamers obtained from FO-SPR measurements was compared for both interfacial architectures. From Figure 6B, it can be noticed that the architecture incorporating of PLL-DBCO increases the amount of the immobilized HD22 aptamer (obtained from FO-SPR measurements) compared to the direct clicking of DBCO-HD22 by 29%.

In addition, the K_D values obtained from the Hill (n = 1) fitting of the response of both OECTs toward thrombin were compared. From Figure 6C, it can be observed that the obtained K_D for the PLL-DBCO-functionalized OECTs is comparable to that obtained for DBCO-HD22-functionalized PEDOT-N_3 OECTs, showing that the binding of thrombin to the HD22 aptamer exosite is not affected by the substitution of the DBCO-terminal group by a N_3 terminal group.

Next, the maximum change in the registered I_{DS} (obtained for the thrombin solution of 400 nM) was also analyzed for both interfacial architectures (Figure 6D). It is observed that the transistors modified with PLL-DBCO and subsequently with the N_3-aptamer showed a higher maximum I_{DS} change by 19%. The higher density of the immobilized HD22 aptamer determined by FO-SPR can be ascribed as one of the reasons

https://doi.org/10.1021/acsami.2c21493
ACS Appl. Mater. Interfaces 2023, 15, 10885−10896

for the better performance of the PLL-based biosensing platforms.

On the other hand, the grafted OEG moieties to PLL could prevent nonspecific binding, which (also) greatly influences the response of the biosensing devices.[42] The use of PEG-PLL has been reported as the most employed and cost-effective approach to functionalize surfaces and provide them with uniform antifouling features.[40] Previous works have shown the inhibition of unspecific binding of proteins such as myoglobin, albumin, and fibrinogen as well as serum fouling.[64,65] Therefore, the incorporation of antifouling properties to the sensing interface prevents the arising of signals ascribed to nonspecific adsorption, therefore improving the specificity of the developed biosensors and yielding a higher change in the recorded signal.

In this regard, while the DBCO-HD22-based architecture showed a higher surface density of recognized thrombin (193 ± 25 ng/cm^2 vs 151 ± 22 ng/cm^2),[23] the maximum I_{DS} change registered by the OECTs functionalized with PLL-DBCO and N_3-HD22 is higher, supporting this hypothesis.

In conclusion, the results presented above show that the developed PLL-DBCO-based approach involves a novel and effective way to immobilize aptamers to PEDOT-N_3 OECTs and construct sensitive thrombin detecting devices. The incorporation of the antifouling OEG moieties in the PLL polymer combined with the specific recognition features of the HD22 aptamer and the accurate signal transduction by the organic transistor operating at low voltages make up for an elegant and effective biosensing interface.

CONCLUSIONS

We have explored different aspects of the interface functionalization of "clickable" OECTs. First, upon studying different channel architectures, it was shown that a PEDOT-N_3 layer is sufficiently conducting to obtain proper functioning OECTs. Next, the clicking of redox probes under different conditions allowed the spatial control of the functionalization, and the Cu(I)-free clicking of PLL-DBCO was also demonstrated. The functionalization with PLL-DBCO allowed further immobilization of a HD22 aptamer, which endowed the fabrication of thrombin recognition devices with antifouling features. Compared to previously reported architectures, the developed sensors showed higher density of immobilized aptamer, which was translated in the biosensor's response as a higher maximum obtained signal change upon analyte recognition.

We believe that this work can pave the way toward the development of efficient OECT-based biosensing devices based on click chemistry functionalization. Further experiments will be directed toward the evaluation of the sensing features of the functionalized OECTs in minimally processed real samples, such as diluted blood or serum, with the aim of developing a label-free point-of-care biosensing device that does not require pre-separation steps.

ASSOCIATED CONTENT

Supporting Information

The Supporting Information is available free of charge at https://pubs.acs.org/doi/10.1021/acsami.2c21493.

Materials and Methods section, synthesis of EDOT-N_3 and PLL-DBCO details, comparison of the OECT fabrication protocols, control experiments for the clicking of redox probes and aptamers, FO-SPR, EIS, CV, and further measurements (PDF)

AUTHOR INFORMATION

Corresponding Authors

Gonzalo E. Fenoy − *AIT Austrian Institute of Technology GmbH, 3430 Tulln an der Donau, Austria; Instituto de Investigaciones Fisicoquímicas Teóricas y Aplicadas (INIFTA), Departamento de Química, Facultad de Ciencias Exactas, Universidad Nacional de La Plata (UNLP)—CONICET, 1900 La Plata, Argentina;* orcid.org/0000-0003-4336-4843; Email: Gonzalo.Fenoy@ait.ac.at

Omar Azzaroni − *Instituto de Investigaciones Fisicoquímicas Teóricas y Aplicadas (INIFTA), Departamento de Química, Facultad de Ciencias Exactas, Universidad Nacional de La Plata (UNLP)—CONICET, 1900 La Plata, Argentina; CEST-UNLP Partner Lab for Bioelectronics (INIFTA), 1900 La Plata, Argentina;* orcid.org/0000-0002-5098-0612; Email: omarazzaroni@quimica.unlp.edu.ar

Wolfgang Knoll − *AIT Austrian Institute of Technology GmbH, 3430 Tulln an der Donau, Austria; Danube Private University, 3500 Krems, Austria;* orcid.org/0000-0003-1543-4090; Email: Wolfgang.Knoll@ait.ac.at

Authors

Roger Hasler − *AIT Austrian Institute of Technology GmbH, 3430 Tulln an der Donau, Austria;* orcid.org/0000-0002-0883-3053

Christoph Lorenz − *Institute for Organic Chemistry II and Advanced Materials, University of Ulm, 89081 Ulm, Germany*

Jacopo Movilli − *Department of Molecules & Materials, MESA+ Institute, Faculty of Science and Technology, University of Twente, AE 7500 Enschede, The Netherlands*

Waldemar A. Marmisollé − *Instituto de Investigaciones Fisicoquímicas Teóricas y Aplicadas (INIFTA), Departamento de Química, Facultad de Ciencias Exactas, Universidad Nacional de La Plata (UNLP)—CONICET, 1900 La Plata, Argentina;* orcid.org/0000-0003-0031-5371

Jurriaan Huskens − *Department of Molecules & Materials, MESA+ Institute, Faculty of Science and Technology, University of Twente, AE 7500 Enschede, The Netherlands;* orcid.org/0000-0002-4596-9179

Peter Bäuerle − *Institute for Organic Chemistry II and Advanced Materials, University of Ulm, 89081 Ulm, Germany;* orcid.org/0000-0003-2017-4414

Complete contact information is available at: https://pubs.acs.org/10.1021/acsami.2c21493

Author Contributions

The manuscript was written through contributions of all authors. All authors have given approval to the final version of the manuscript.

Funding

W.A.M. and O.A. are staff members of CONICET. G.E.F. acknowledges CONICET for a postdoctoral fellowship. This study was supported by the Netherlands Organization for Scientific Research (NWO, TOP grant 715.015.001 to J.H.). This project has received funding from the European Union's Horizon 2020 Research and Innovation Programme under the

Marie Skłodowska-Curie grant agreement no. 813863-BORGES.

Notes

The authors declare no competing financial interest.

Data Availability: The data that support the findings of this study are openly available in Zenodo (DOI: https://doi.org/10.5281/zenodo.7215842).

■ ACKNOWLEDGMENTS

R.H. thanks the group of Prof. Maria Ibáñez and the Electron Microscopy Facility at the Institute of Science and Technology Austria (ISTA).

■ REFERENCES

(1) Rivnay, J.; Inal, S.; Salleo, A.; Owens, R. M.; Berggren, M.; Malliaras, G. G. Organic Electrochemical Transistors. *Nat. Rev. Mater.* **2018**, *3*, 17086.

(2) Rashid, R. B.; Ji, X.; Rivnay, J. Organic Electrochemical Transistors in Bioelectronic Circuits. *Biosens. Bioelectron.* **2021**, *190*, 113461.

(3) Khodagholy, D.; Gurfinkel, M.; Stavrinidou, E.; Leleux, P.; Herve, T.; Sanaur, S.; Malliaras, G. G. High Speed and High Density Organic Electrochemical Transistor Arrays. *Appl. Phys. Lett.* **2011**, *99*, 163304.

(4) Yang, S. Y.; DeFranco, J. A.; Sylvester, Y. A.; Gobert, T. J.; Macaya, D. J.; Owens, R. M.; Malliaras, G. G. Integration of a Surface-Directed Microfluidic System with an Organic Electrochemical Transistor Array for Multi-Analyte Biosensors. *Lab Chip* **2009**, *9*, 704−708.

(5) Nawaz, A.; Liu, Q.; Leong, W. L.; Fairfull-Smith, K. E.; Sonar, P. Organic Electrochemical Transistors for In Vivo Bioelectronics. *Adv. Mater.* **2021**, *33*, 2170387.

(6) Marks, A.; Griggs, S.; Gasparini, N.; Moser, M. Organic Electrochemical Transistors: An Emerging Technology for Biosensing. *Adv. Mater. Interfaces* **2022**, *9*, 2102039.

(7) Cucchi, M.; Kleemann, H.; Tseng, H.; Ciccone, G.; Lee, A.; Pohl, D.; Leo, K. Directed Growth of Dendritic Polymer Networks for Organic Electrochemical Transistors and Artificial Synapses. *Adv. Electron. Mater.* **2021**, *7*, 2100586.

(8) Fenoy, G. E.; Azzaroni, O.; Knoll, W.; Marmisollé, W. A. Functionalization Strategies of PEDOT and PEDOT:PSS Films for Organic Bioelectronics Applications. *Chemosensors* **2021**, *9*, 212.

(9) Inal, S.; Malliaras, G. G.; Rivnay, J. Benchmarking Organic Mixed Conductors for Transistors. *Nat. Commun.* **2017**, *8*, 1767.

(10) Keene, S. T.; Pol, T. P. A.; Zakhidov, D.; Weijtens, C. H. L.; Janssen, R. A. J.; Salleo, A.; Burgt, Y. Enhancement-Mode PEDOT:PSS Organic Electrochemical Transistors Using Molecular De-Doping. *Adv. Mater.* **2020**, *32*, 2000270.

(11) Fenoy, G. E.; Bilderling, C.; Knoll, W.; Azzaroni, O.; Marmisollé, W. A. PEDOT:Tosylate-Polyamine-Based Organic Electrochemical Transistors for High-Performance Bioelectronics. *Adv. Electron. Mater.* **2021**, *7*, 2100059.

(12) Fenoy, G. E.; Scotto, J.; Allegretto, J. A.; Piccinini, E.; Cantillo, A. L.; Knoll, W.; Azzaroni, O.; Marmisollé, W. A. Layer-by-Layer Assembly Monitored by PEDOT-Polyamine-Based Organic Electrochemical Transistors. *ACS Appl. Electron. Mater.* **2022**, *4*, 5953−5962.

(13) Donahue, M. J.; Sanchez-Sanchez, A.; Inal, S.; Qu, J.; Owens, R. M.; Mecerreyes, D.; Malliaras, G. G.; Martin, D. C. Tailoring PEDOT Properties for Applications in Bioelectronics. *Mater. Sci. Eng., R* **2020**, *140*, 100546.

(14) Huang, L.; Yang, X.; Deng, L.; Ying, D.; Lu, A.; Zhang, L.; Yu, A.; Duan, B. Biocompatible Chitin Hydrogel Incorporated with PEDOT Nanoparticles for Peripheral Nerve Repair. *ACS Appl. Mater. Interfaces* **2021**, *13*, 16106−16117.

(15) Hopkins, J.; Fidanovski, K.; Travaglini, L.; Ta, D.; Hook, J.; Wagner, P.; Wagner, K.; Lauto, A.; Cazorla, C.; Officer, D.; Mawad, D. A Phosphonated Poly(Ethylenedioxythiophene) Derivative with Low Oxidation Potential for Energy-Efficient Bioelectronic Devices. *Chem. Mater.* **2022**, *34*, 140−151.

(16) Minudri, D.; Mantione, D.; Dominguez-Alfaro, A.; Moya, S.; Maza, E.; Bellacanzone, C.; Antognazza, M. R.; Mecerreyes, D. Water Soluble Cationic Poly(3,4-Ethylenedioxythiophene) PEDOT-N as a Versatile Conducting Polymer for Bioelectronics. *Adv. Electron. Mater.* **2020**, *6*, 2000510.

(17) Elschner, A.; Kirchmeyer, S.; Lövenich, W.; Merker, U.; Reuter, K. *PEDOT: Principles and Applications of an Intrinsically Conductive Polymer*; CRC Press, 2010.

(18) Daugaard, A. E.; Hvilsted, S.; Hansen, T. S.; Larsen, N. B. Conductive Polymer Functionalization by Click Chemistry. *Macromolecules* **2008**, *41*, 4321−4327.

(19) Bu, H. B.; Götz, G.; Reinold, E.; Vogt, A.; Schmid, S.; Blanco, R.; Segura, J. L.; Bäuerle, P. "Click"-functionalization of conducting poly(3,4-ethylenedioxythiophene) (PEDOT). *Chem. Commun.* **2008**, *11*, 1320−1322.

(20) Attar, A. M.; Richardson, M. B.; Speciale, G.; Majumdar, S.; Dyer, R. P.; Sanders, E. C.; Penner, R. M.; Weiss, G. A. Electrochemical Quantification of Glycated and Non-Glycated Human Serum Albumin in Synthetic Urine. *ACS Appl. Mater. Interfaces* **2019**, *11*, 4757−4765.

(21) Sitarik, P.; Nagane, S. S.; Chhatre, S.; Wu, Y.; Baugh, Q.; Martin, D. C. Synthesis and Characterization of Maleimide Functionalized Poly(3,4-Ethylenedioxythiophene) (PEDOT) Polymers. *Mater. Adv.* **2022**, *3*, 6037−6049.

(22) Khau, B. V.; Savagian, L. R.; De Keersmaecker, M.; Gonzalez, M. A.; Reichmanis, E. Carboxylic Acid Functionalization Yields Solvent-Resistant Organic Electrochemical Transistors. *ACS Mater. Lett.* **2019**, *1*, 599−605.

(23) Fenoy, G. E.; Hasler, R.; Quartinello, F.; Marmisollé, W. A.; Lorenz, C.; Azzaroni, O.; Bäuerle, P.; Knoll, W. "Clickable" Organic Electrochemical Transistors. *JACS Au* **2022**, *2*, 2778−2790.

(24) Xi, W.; Scott, T. F.; Kloxin, C. J.; Bowman, C. N. Click Chemistry in Materials Science. *Adv. Funct. Mater.* **2014**, *24*, 2572−2590.

(25) NobelPrize.org. *The Nobel Prize in Chemistry 2022*. Nobel Prize Outreach AB 2022, 2022. https://www.nobelprize.org/prizes/chemistry/2022/press-release/.

(26) Degirmenci, A.; Yeter Bas, G.; Sanyal, R.; Sanyal, A. "Clickable" Polymer Brush Interfaces: Tailoring Monovalent to Multivalent Ligand Display for Protein Immobilization and Sensing. *Bioconjugate Chem.* **2022**, *33*, 1672.

(27) Kaur, J.; Saxena, M.; Rishi, N. An Overview of Recent Advances in Biomedical Applications of Click Chemistry. *Bioconjugate Chem.* **2021**, *32*, 1455−1471.

(28) Moses, J. E.; Moorhouse, A. D.; Moses, J. E.; Sharpless, K. B. The growing applications of click chemistry. *Chem. Soc. Rev.* **2007**, *36*, 1249−1262.

(29) Presolski, S. I.; Hong, V. P.; Finn, M. G. Copper-Catalyzed Azide-Alkyne Click Chemistry for Bioconjugation. *Curr. Protoc. Chem. Biol.* **2011**, *3*, 153−162.

(30) Chen, Y.; Xianyu, Y.; Wu, J.; Yin, B.; Jiang, X. Click Chemistry-Mediated Nanosensors for Biochemical Assays. *Theranostics* **2016**, *6*, 969−985.

(31) Yáñez-Sedeño, P.; González-Cortés, A.; Campuzano, S.; Pingarrón, J. M. Copper(I)-Catalyzed Click Chemistry as a Tool for the Functionalization of Nanomaterials and the Preparation of Electrochemical (Bio)Sensors. *Sensors* **2019**, *19*, 2379.

(32) Di Iorio, D.; Rameshbabu, S.; Bruijns, B.; Movilli, J.; Skolimowski, M.; Huskens, J. Click-and-Bond: Room-Temperature and Solvent-Free Bonding of Polymer-Based Microfluidic Devices. *Adv. Mater. Interfaces* **2022**, *9*, 2200282.

(33) Nerantzaki, M.; Loth, C.; Lutz, J. F. Chemical Conjugation of Nucleic Acid Aptamers and Synthetic Polymers. *Polym. Chem.* **2021**, *12*, 3498−3509.

(34) Becer, C.; Hoogenboom, R.; Schubert, U. S. Click Chemistry beyond Metal-Catalyzed Cycloaddition. *Angew. Chem., Int. Ed.* **2009**, *48*, 4900−4908.

(35) Shavokshina, V. A.; Komkova, M. A.; Aparin, I. O.; Zatsepin, T. S.; Karyakin, A. A.; Andreev, E. A. Improved Electroactivity of Redox Probes onto Electropolymerized Azidomethyl-PEDOT: Enabling Click Chemistry for Advanced (Bio)Sensors. *ACS Appl. Polym. Mater.* **2021**, *3*, 1518−1524.
(36) Mishyn, V.; Rodrigues, T.; Leroux, Y. R.; Aspermair, P.; Happy, H.; Bintinger, J.; Kleber, C.; Boukherroub, R.; Knoll, W.; Szunerits, S. Controlled Covalent Functionalization of a Graphene-Channel of a Field Effect Transistor as an Ideal Platform for (Bio)Sensing Applications. *Nanoscale Horiz.* **2021**, *6*, 819−829.
(37) Fenoy, G. E.; Marmisollé, W. A.; Azzaroni, O.; Knoll, W. Acetylcholine Biosensor Based on the Electrochemical Functionalization of Graphene Field-Effect Transistors. *Biosens. Bioelectron.* **2020**, *148*, 111796.
(38) Fenoy, G. E.; Marmisollé, W. A.; Knoll, W.; Azzaroni, O. Highly Sensitive Urine Glucose Detection with Graphene Field-Effect Transistors Functionalized with Electropolymerized Nanofilms. *Sens. Diagn.* **2022**, *1*, 139−148.
(39) Fenoy, G. E.; Piccinini, E.; Knoll, W.; Marmisollé, W. A.; Azzaroni, O. The Effect of Amino-Phosphate Interactions on the Biosensing Performance of Enzymatic Graphene Field-Effect Transistors. *Anal. Chem.* **2022**, *94*, 13820−13828.
(40) Movilli, J.; Huskens, J. Functionalized Polyelectrolytes for Bioengineered Interfaces and Biosensing Applications. *Org. Mater.* **2020**, *02*, 078−107.
(41) Bellassai, N.; D'Agata, R.; Marti, A.; Rozzi, A.; Volpi, S.; Allegretti, M.; Corradini, R.; Giacomini, P.; Huskens, J.; Spoto, G. Detection of Tumor DNA in Human Plasma with a Functional PLL-Based Surface Layer and Plasmonic Biosensing. *ACS Sens.* **2021**, *6*, 2307−2319.
(42) Movilli, J.; Rozzi, A.; Ricciardi, R.; Corradini, R.; Huskens, J. Control of Probe Density at DNA Biosensor Surfaces Using Poly(l-lysine) with Appended Reactive Groups. *Bioconjugate Chem.* **2018**, *29*, 4110−4118.
(43) Di Iorio, D.; Marti, A.; Koeman, S.; Huskens, J. Clickable Poly-l-Lysine for the Formation of Biorecognition Surfaces. *RSC Adv.* **2019**, *9*, 35608−35613.
(44) Hasler, R.; Reiner-Rozman, C.; Fossati, S.; Aspermair, P.; Dostalek, J.; Lee, S.; Ibáñez, M.; Bintinger, J.; Knoll, W. Field-Effect Transistor with a Plasmonic Fiber Optic Gate Electrode as a Multivariable Biosensor Device. *ACS Sens.* **2022**, *7*, 504−512.
(45) Bandyopadhyay, S.; Mukherjee, S.; Dey, A. Modular Synthesis, Spectroscopic Characterization and in Situ Functionalization Using "Click" Chemistry of Azide Terminated Amide Containing Self-Assembled Monolayers. *RSC Adv.* **2013**, *3*, 17174−17187.
(46) Fenoy, G. E.; Rafti, M.; Marmisollé, W. A.; Azzaroni, O. Nanoarchitectonics of Metal Organic Frameworks and PEDOT Layer-by-Layer Electrodes for Boosting Oxygen Reduction Reaction. *Mater. Adv.* **2021**, *2*, 7731−7740.
(47) Gu, M.; Travaglini, L.; Hopkins, J.; Ta, D.; Lauto, A.; Wagner, P.; Wagner, K.; Zeglio, E.; Jephcott, L.; Officer, D. L.; Mawad, D. Molecular Design of an Electropolymerized Copolymer with Carboxylic and Sulfonic Acid Functionalities. *Synth. Met.* **2022**, *285*, 117029.
(48) Musumeci, C.; Hutchison, J. A.; Samorì, P. Controlling the Morphology of Conductive PEDOT by in Situ Electropolymerization: From Thin Films to Nanowires with Variable Electrical Properties. *Nanoscale* **2013**, *5*, 7756−7761.
(49) Rivnay, J.; Leleux, P.; Sessolo, M.; Khodagholy, D.; Hervé, T.; Fiocchi, M.; Malliaras, G. G. Organic Electrochemical Transistors with Maximum Transconductance at Zero Gate Bias. *Adv. Mater.* **2013**, *25*, 7010−7014.
(50) Lind, J. U.; Hansen, T. S.; Daugaard, A. E.; Hvilsted, S.; Andresen, T. L.; Larsen, N. B. Solvent Composition Directing Click-Functionalization at the Surface or in the Bulk of Azide-Modified PEDOT. *Macromolecules* **2011**, *44*, 495−501.
(51) Valincius, G.; Niaura, G.; Kazakevičienė, B.; Talaikytė, Z.; Kažemėkaitė, M.; Butkus, E.; Razumas, V. Anion Effect on Mediated Electron Transfer through Ferrocene-Terminated Self-Assembled Monolayers. *Langmuir* **2004**, *20*, 6631−6638.
(52) Sumner, J. J.; Creager, S. E. Redox Kinetics in Monolayers on Electrodes: Electron Transfer Is Sluggish for Ferrocene Groups Buried within the Monolayer Interior. *J. Phys. Chem. B* **2001**, *105*, 8739−8745.
(53) Bellassai, N.; Marti, A.; Spoto, G.; Huskens, J. Low-Fouling, Mixed-Charge Poly-l-Lysine Polymers with Anionic Oligopeptide Side-Chains. *J. Mater. Chem. B* **2018**, *6*, 7662−7673.
(54) Han, Z.; Wang, Y.; Duan, X. Biofunctional polyelectrolytes assembling on biosensors - A versatile surface coating method for protein detections. *Anal. Chim. Acta* **2017**, *964*, 170−177.
(55) Wu, Z. S.; Parvez, K.; Winter, A.; Vieker, H.; Liu, X.; Han, S.; Turchanin, A.; Feng, X.; Müllen, K. Layer-by-Layer Assembled Heteroatom-Doped Graphene Films with Ultrahigh Volumetric Capacitance and Rate Capability for Micro-Supercapacitors. *Adv. Mater.* **2014**, *26*, 4552−4558.
(56) Wang, J.; Zhang, S.; Zhang, Y. Fabrication of Chronocoulometric DNA Sensor Based on Gold Nanoparticles/Poly(l-Lysine) Modified Glassy Carbon Electrode. *Anal. Biochem.* **2010**, *396*, 304−309.
(57) Derszniak, K.; Przyborowski, K.; Matyjaszczyk, K.; Moorlag, M.; de Laat, B.; Nowakowska, M.; Chlopicki, S. Comparison of Effects of Anti-Thrombin Aptamers HD1 and HD22 on Aggregation of Human Platelets, Thrombin Generation, Fibrin Formation, and Thrombus Formation Under Flow Conditions. *Front. Pharmacol.* **2019**, *10*, 68.
(58) Mann, K. G.; Brummel, K.; Butenas, S. What Is All That Thrombin For? *J. Thromb. Haemostasis* **2003**, *1*, 1504−1514.
(59) Crawley, J. T. B.; Zanardelli, S.; Chion, C. K. N. K.; Lane, D. A. The Central Role of Thrombin in Hemostasis. *J. Thromb. Haemostasis* **2007**, *5*, 95−101.
(60) Yousef, H.; Liu, Y.; Zheng, L. Nanomaterial-Based Label-Free Electrochemical Aptasensors for the Detection of Thrombin. *Biosensors* **2022**, *12*, 253.
(61) Kotlarek, D.; Curti, F.; Vorobii, M.; Corradini, R.; Careri, M.; Knoll, W.; Rodriguez-Emmenegger, C.; Dostálek, J. Surface Plasmon Resonance-Based Aptasensor for Direct Monitoring of Thrombin in a Minimally Processed Human Blood. *Sens. Actuators, B* **2020**, *320*, 128380.
(62) Hammock, M. L.; Knopfmacher, O.; Naab, B. D.; Tok, J. B. H.; Bao, Z. Investigation of Protein Detection Parameters Using Nanofunctionalized Organic Field-Effect Transistors. *ACS Nano* **2013**, *7*, 3970−3980.
(63) Lin, P. H.; Chen, R. H.; Lee, C. H.; Chang, Y.; Chen, C. S.; Chen, W. Y. Studies of the Binding Mechanism between Aptamers and Thrombin by Circular Dichroism, Surface Plasmon Resonance and Isothermal Titration Calorimetry. *Colloids Surf., B* **2011**, *88*, 552−558.
(64) Lee, S.; Vörös, J. An Aqueous-Based Surface Modification of Poly(Dimethylsiloxane) with Poly(Ethylene Glycol) to Prevent Biofouling. *Langmuir* **2005**, *21*, 11957−11962.
(65) Michel, R.; Pasche, S.; Textor, M.; Castner, D. G. Influence of PEG Architecture on Protein Adsorption and Conformation. *Langmuir* **2005**, *21*, 12327−12332.

https://doi.org/10.1021/acsami.2c21493
ACS Appl. Mater. Interfaces 2023, 15, 10885−10896